The tethering function of mitofusin2 controls osteoclast differentiation by modulating the Ca^{2+}–NFATc1 axis

Received for publication, November 25, 2019, and in revised form, March 6, 2020 Published, Papers in Press, March 12, 2020, DOI 10.1074/jbc.RA119.012023

Anna Ballard[‡§], Rong Zeng[‡§], Allahdad Zarei[‡§], Christine Shao[‡§], Linda Cox[‡§], Hui Yan[§¶‖], Antonietta Franco[**], Gerald W. Dorn II[**], Roberta Faccio[§¶‡‡], and Deborah J. Veis[‡§‡‡§§1]

*From the [‡]Division of Bone and Mineral Diseases, Department of Medicine, Washington University School of Medicine, St. Louis, Missouri 63110, the [§]Musculoskeletal Research Center, Washington University School of Medicine, St. Louis, Missouri 63110, the [¶]Department of Orthopedic Surgery, Washington University School of Medicine, St. Louis, Missouri 63110, the [‖]Animal Nutrition Institute, Sichuan Agricultural University, Chengdu 611130, China, the **Center for Pharmacogenomics, Department of Medicine, Washington University School of Medicine, St. Louis, Missouri 63110, [‡‡]Shriners Hospitals for Children, St. Louis, Missouri 63110 and the [§§]Department of Pathology and Immunology, Washington University School of Medicine, St. Louis, Missouri 63110*

Edited by John M. Denu

Dynamic regulation of the mitochondrial network by mitofusins (MFNs) modulates energy production, cell survival, and many intracellular signaling events, including calcium handling. However, the relative importance of specific mitochondrial functions and their dependence on MFNs vary greatly among cell types. Osteoclasts have many mitochondria, and increased mitochondrial biogenesis and oxidative phosphorylation enhance bone resorption, but little is known about the mitochondrial network or MFNs in osteoclasts. Because expression of each MFN isoform increases with osteoclastogenesis, we conditionally deleted MFN1 and MFN2 (double conditional KO (dcKO)) in murine osteoclast precursors, finding that this increased bone mass in young female mice and abolished osteoclast precursor differentiation into mature osteoclasts *in vitro*. Defective osteoclastogenesis was reversed by overexpression of MFN2 but not MFN1; therefore, we generated mice lacking only MFN2 in osteoclasts. MFN2-deficient female mice had increased bone mass at 1 year and resistance to Receptor Activator of NF-κB Ligand (RANKL)-induced osteolysis at 8 weeks. To explore whether MFN-mediated tethering or mitophagy is important for osteoclastogenesis, we overexpressed MFN2 variants defective in either function in dcKO precursors and found that, although mitophagy was dispensable for differentiation, tethering was required. Because the master osteoclastogenic transcriptional regulator nuclear factor of activated T cells 1 (NFATc1) is calcium-regulated, we assessed calcium release from the endoplasmic reticulum and store-operated calcium entry and found that the latter was blunted in dcKO cells. Restored osteoclast differentiation by expression of intact MFN2 or the mitophagy-defective variant was associated with normalization of store-operated calcium entry and NFATc1 levels, indicating that MFN2 controls mitochondrion–endoplasmic reticulum tethering in osteoclasts.

Mitochondria exist within a highly regulated and dynamic network in most cell types. Termed mitochondrial dynamics, the linked processes of fission, fusion, and mitophagy play an important role in mitochondrial homeostasis. Changes in mitochondrial networks are frequent, and this architecture varies depending on the developmental or metabolic needs of a cell (reviewed in Refs. 1, 2). Mitofusin1 (MFN1)[2] and Mitofusin2 (MFN2), transmembrane GTPases on the outer mitochondrial membrane, control mitochondrial architecture by tethering adjacent mitochondria and initiating fusion. MFN2 additionally mediates tethering of mitochondria to the ER, promotes mitophagy, and allows mitochondrial transport down axons. MFN1 and MFN2 are necessary for survival, as global deletion of either protein results in embryonic lethality prior to embryonic day 12.5 in mice (3). Double deletion of MFN1 and MFN2 leads to even earlier mortality and, in mouse embryonic fibroblasts, causes severe fragmentation of mitochondrial networks (3).

In humans, the nervous system is highly impacted by MFN2 defects, and *MFN2* mutations are linked to neuropathies (reviewed in Refs. 4, 5). The human syndrome most associated with mutations in *MFN2* is Charcot–Marie–Tooth type 2A

This work was supported by NIAMS, National Institutes of Health Grants R01 AR052705 (to D. J. V.) and R01 AR070030 (to D. J. V. and R. F.) and R01 AR066551 (to R. F.), funding from Shriners Hospitals for Children (to D. J. V. and R. F.), as well as NIAMS, National Institutes of Health Metabolic Skeletal Disorders Training Program Grant T32AR060719 (to A. B. and R. Z.). Slide scanning was made possible with support from a Hope Center for Neurological Disorders shared instrumentation grant (NCRR, National Institutes of Health Grant 1S10RR027552) and μCT and histology by a Musculoskeletal Research Center grant (NIAMS, National Institutes of Health Grant P30 AR074992 (to R. F. and D. J. V.). G. W. D. is a founder of Mitochondria in Motion, Inc., a St. Louis–based startup biotech R&D company focused on enhancing mitochondrial trafficking and fitness in neurodegenerative diseases, and may financially benefit if the company is successful in marketing products related to this research. The content is solely the responsibility of the authors and does not necessarily represent the official views of the National Institutes of Health.

This article contains Figs. S1–S4 and Table S1.

[1] To whom correspondence should be addressed: Washington University School of Medicine, Dept. of Medicine, Division of Bone and Mineral Diseases, 660 S. Euclid Ave., Campus Box 8301, St. Louis, MO 63110. Tel.: 314-454-8472; E-mail: dveis@wustl.edu.

[2] The abbreviations used are: Mfn, Mitofusin; ER, endoplasmic reticulum; CMT2A, Charcot–Marie–Tooth type 2A; OC, osteoclast; BMM, bone marrow macrophage; dcKO, double conditional KO; ctrl, control; BV, bone volume; TV, total volume; BMD, bone mineral density; V, vector; SOCE, store-operated calcium entry; RANKL, receptor activator of NF-κB ligand; M-CSF, macrophage-colony stimulating factor; TRAP, tartrate resistant acid phosphatase; Cort.Th, cortical thickness; BS, bone surface.

(CMT2A), a neurodegenerative disorder in which motor and sensory defects develop within the first two decades of life (6). Mice with homologous *Mfn2* mutations have sensory and/or motor defects and axonal degeneration accompanied by altered mitochondrial dynamics (7–9), and cultured human cells from CMT2A patients display decreased electrical properties and reduced mitochondrial membrane potential (10, 11). Models lacking mitofusins also yield conditions of myocardial hypertrophy, heart tube contractile dysfunction, vascular smooth muscle cell proliferation, and skeletal muscle atrophy, to name a few (12–15). To our knowledge, effects on the skeleton have not been reported in CMT2A mouse models or human patients. Additionally, no human syndromes with *MFN1* mutations have been described.

Bone homeostasis relies on the coupled activity of osteoblast and osteoclast (OC) cells that build and resorb the bone matrix, respectively. OCs are rich in mitochondria, and differentiation from bone marrow macrophage (BMM) precursors to OCs is associated with a significant increase in mitochondrial DNA copy number, oxidative phosphorylation subunit protein levels, and oxygen consumption rates (16). Previous investigations of mitochondria in the OC lineage have largely focused on the role of mitochondrial biogenesis and oxidative phosphorylation in supporting OC function (17–19). We were prompted to explore the role of mitochondrial dynamics in OCs because this specialized cell type is mitochondrion-rich and undergoes vast morphological changes to become a mature multinucleated cell. We hypothesized that mitochondrial fusion might accompany OC precursor fusion during osteoclastogenesis and that tethering of mitochondria to each other or the ER is important for OC formation and/or function. To test this, we generated a mouse model in which MFN1 and MFN2 are conditionally deleted in the OC lineage with LysM-cre. We found that knockout of both homologs is associated with increased bone mass in female animals and blunted osteoclastogenesis in culture. Rescue experiments *in vitro* revealed that MFN2 more strongly induces osteoclastogenesis than MFN1 and that *in vivo*, depletion of MFN2 is protective against age- and RANKL-induced bone loss. Last, we demonstrate mitochondrial tethering to be the predominant function of MFN2 in OCs, associated with changes in Ca^{2+}–NFATc1 signaling.

Results

Bone mass is increased in female mice lacking MFN1 and MFN2 in the OC lineage

Because OCs undergo vast morphological changes to become mature multinucleated cells, we hypothesized that alterations in mitochondrial dynamics, and fusion in particular, accompany and modulate this event. To prevent mitochondrial fusion, we employed mice with floxed alleles for both *Mfn1* and *Mfn2*, directing their excision to the OC lineage with LysM-cre. All of our mice were mated onto a homozygous cre background ($LysM^{c/c}$) to increase recombination efficiency. We intercrossed double heterozygous ($LysM^{c/c}$; $(Mfn1/2)^{fl/+}$ = ctrl) mice to generate double knockout ($LysM^{c/c}$; $(Mfn1/2)^{fl/fl}$; dcKO) littermates, which were born at normal Mendelian ratios. Subsequently, these dcKO progeny were mated to the double-heterozygous ctrl mice to produce our experimental groups. In parallel, double heterozygous ctrl mice were bred to cre-only ($LysM^{c/c}$;$(Mfn1/2)^{+/+}$) mice to generate a cohort of ctrl and cre-only littermates. Importantly, there was no difference in bone mass parameters between ctrl and cre-only groups (Fig. S1, *A–N*), indicating that ctrl double-heterozygous animals are an appropriate control group for dcKO mice.

dcKO mice showed no obvious gross phenotypes and had weights identical to ctrl littermates (Fig. S2, *A* and *B*). Male and female animals were sacrificed at 2 months of age, a time of high OC activity, and basal bone morphology was assessed by μCT of dissected femora. We found a strong bone phenotype in female animals at this age, with all trabecular and cortical parameters consistent with a high bone mass (significantly increased bone volume (BV) per total volume (TV), bone mineral density (BMD), trabecular number (Tb.N), and cortical thickness (Cort.Th)) (Fig. 1, *A* and *B*, and Fig. S2, *C–F*). Interestingly, males showed no significant differences between ctrl and dcKO groups in any of these parameters (Fig. 1, *C* and *D*, and Fig. S2, *G–J*). Serum CTX-1 levels were decreased in dcKO females, indicating a decrease in bone catabolism (Fig. 2*A*). Histomorphometry showed that OC surface and number in dcKOs trended lower than in ctrls in female mice (Fig. 2, *B–E*). Osteoblast–OC coupling was not affected by loss of MFN1 and MFN2 in OCs; indices of bone formation, such as serum P1NP, mineralizing surface, mineral apposition rate, and bone formation rate, were unchanged between groups (Fig. 2, *F–K*).

Osteoclastogenesis is inhibited in MFN1/2-deficient cultures

To more closely characterize the impact of mitofusin loss in the OC lineage, BMMs were expanded from bone marrow of ctrl and dcKO mice. Compared with cre-only OCs with WT mitofusin expression, double-heterozygous ctrls produced less MFN1 and MFN2 protein, which was further diminished in dcKO cells (Fig. 3*A*). dcKOs were unable to respond to RANKL and differentiate into OCs on plastic wells, whereas differentiation of ctrls was intact (Fig. 3*B*). When cultured on bone, resorption was also minimal (Fig. 3*C*). Consistently, levels of the OC markers NFATc1, DC-STAMP, and CTSK were reduced in dcKOs at the mRNA level (Fig. 3, *D–F*). Western blots also demonstrated lower levels of Cathepsin K (CTSK) and C-SRC proteins, which supports a defect in OC differentiation (Fig. 3*G*).

The levels of protein and mRNA for both MFN homologs increased throughout osteoclastogenesis in WT cells (Fig. 4, *A* and *B*). Therefore, we sought to determine whether MFN1 or MFN2 was dominant in contributing to the dcKO phenotype and attempted to rescue the defect in OC formation by retrovirally expressing MFN1 or MFN2 in dcKO BMMs. We found that overexpression of MFN2, but not MFN1, restored full OC differentiation, suggesting that MFN2 is the dominant mitofusin homolog that supports osteoclastogenesis (Fig. 4, *C–E*).

MFN2 plays a role in OCs in vivo

To assess whether loss of MFN2 alone in OC lineage cells would have an effect on bone mass *in vivo*, we generated litter-

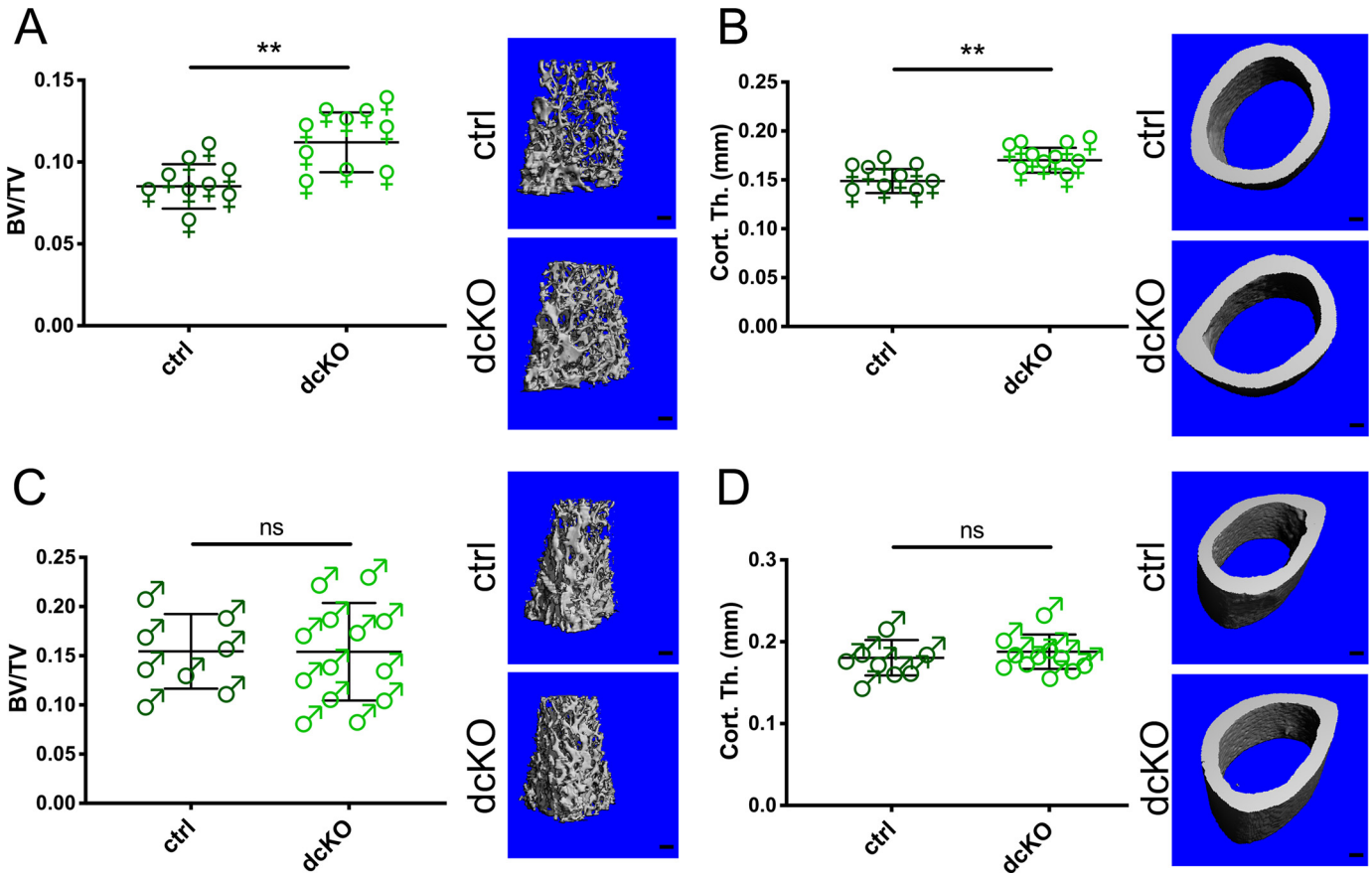

Figure 1. Trabecular and cortical bone mass are increased in 2-month-old female mice lacking MFN1 and MFN2 in the OC lineage. *A* and *B*, BV/TV (*A*) and Cort.Th (*B*) are significantly elevated in female dcKOs compared with ctrls in the distal femur at 2 months of age, as shown by μCT. Representative reconstructions of analyzed regions above the growth plate and at mid-shaft are shown in the *right panels*. *Scale bars* = 200 μm. *C* and *D*, 2-month-old males were evaluated for BV/TV (*C*) and Cort.Th (*D*). **, $p < 0.01$; *ns*, not significant; unpaired *t* test with Welch's correction.

mate cohorts of mice with WT *Mfn2* (*LysM*$^{c/c}$; *Mfn2*$^{+/+}$; cre-only) and conditionally targeted *Mfn2* (*LysM*$^{c/c}$; *Mfn2*$^{fl/fl}$; Mfn2 cKO). We confirmed depletion of MFN2 by evaluating protein and mRNA expression (Fig. 5, *A* and *B*). Although we observed upward trends in female Mfn2 cKOs at 2 and 4 months of age, the differences in BV/TV and BMD did not become statistically significant until 12 months of age; there was no difference in bone mass between male cKO and male cre-only mice at any age examined (Fig. 5, *C–F*, Table 1, and Table S1). The percentage of trabecular bone retained from 4 months to 12 months was 24% for ctrls *versus* 46% for cKO females (64% *versus* 63% for males). Tartrate resistant acid phosphatase (TRAP)-stained 2-month-old tibia sections show a trend toward lower OC number and surface per bone surface (Oc.N/BS and Oc.S/BS) in female cKO mice (Fig. S3). Thus, loss of MFN2 has limited effects on basal bone mass in young animals, whereas it protects female mice from age-related bone loss.

Our group and others have previously observed that challenging animals with a stimulus for pathological bone loss can unmask a robust OC phenotype even when basal changes are not prominent (20–23). We hypothesized that this may be the case for Mfn2 cKO animals and therefore induced acute osteolysis in 2-month-old animals. Male and female cre-only and cKO mice were challenged with intraperitoneal RANKL injection, which stimulates OC activity and induces significant loss of trabecular bone in 2 days. Although cre-only males, male cKOs, and cre-only females lost 30%–45% of trabecular bone fraction following RANKL injection, female cKOs were protected from induced osteolysis, showing no significant change (Fig. 5, *G–I*, and Fig. S4). Therefore, even with a strong OC stimulus, male mice are not affected by loss of MFN2, whereas female mice require MFN2 in the OC to respond.

Mitochondrial tethering is the dominant MFN2 mechanism contributing to osteoclastogenesis in vitro

MFN2 has two primary molecular functions, tethering/fusion and mitophagy, that can be selectively disabled via mutation of threonine and serine residues to constitutively activate or ablate the signal for mitophagy (24). MFN2 T111E-S442E (MFN2-EE) mimics phosphorylation by PINK1 kinase, driving spontaneous mitophagy and preventing fusion, leading to a highly fragmented mitochondrial network. In contrast, MFN2 T111A-S442A (MFN2-AA) has the opposite effect; the non-phosphorylatable MFN2 residues eliminate mitophagy but allow normal tethering and fusion (Fig. 6*A*) (24, 25). To examine the ability of either MFN2 function to impact OCs, we retrovirally overexpressed each mutant, along with empty vector (V) and MFN2-WT controls, in female dcKO BMMs that were defective in producing OCs (Fig. 6*B*). To verify that mutants were functioning properly, we stained transduced BMMs with MitoTracker Green and LysoTracker Red prior to live-cell con-

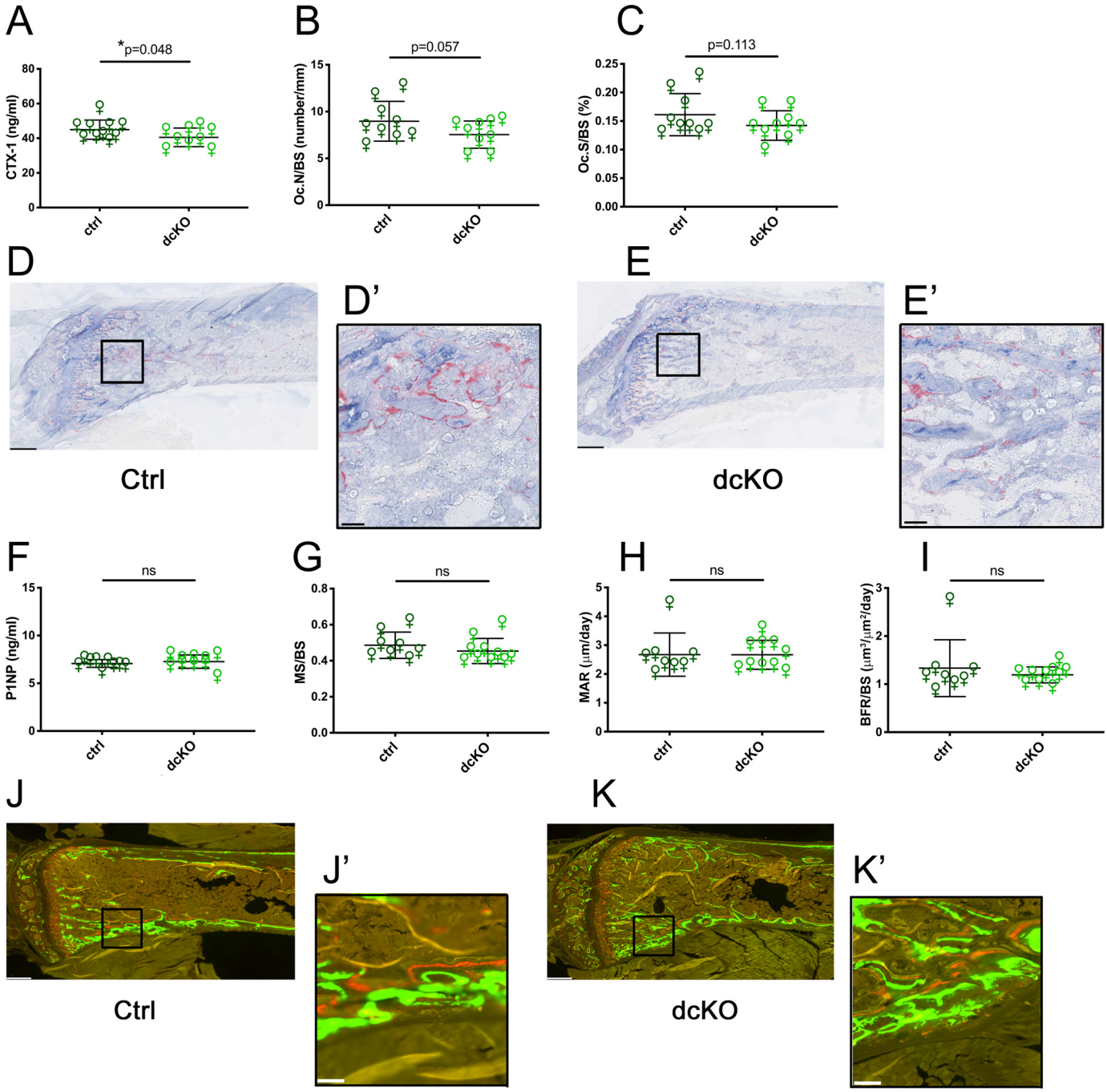

Figure 2. Female Mfn1/2 dcKOs have decreased OC activity but no change in bone formation. *A*, serum CTX-1 assay shows decreased bone resorption in 2-month-old dcKO females. *B* and *C*, histomorphometry of TRAP stained tibiae reveals a modest decreases in dcKO Oc.N/BS (*B*) and Oc.S/BS (*C*). *D* and *E*, representative TRAP-stained ctrl and dcKO femora, respectively. *F–I*, no differences in bone accrual between groups were observed by serum P1NP (*F*) or dynamic histomorphometric analysis of trabecular bone for mineralizing surface (MS)/BS (*G*), mineral apposition rate (MAR) (*H*), and bone formation rate (BFR)/BS (*I*) in tibiae. *J* and *K*, representative fluorescence images of ctrl and dcKO femora, respectively. *Scale bars* = 400 μm (low power) and 40 μm (*insets*). *, $p < 0.05$; *ns*, not significant; one-tailed unpaired *t* test with Welch's correction.

focal microscopy (Fig. 6*C*). Mitochondrial colocalization with lysosomes, an indication of mitophagy, was minimal under all conditions. Similar to previous studies with these constructs, MFN2-WT and MFN2-AA increased tethering and fusion, as manifested by increased mitochondrial aspect ratios (mitochondrial length/mitochondrial width) compared with less fused V and MFN2-EE samples (Fig. 6*D*). Following 6 days of RANKL exposure, cultures were fixed and stained for TRAP (Fig. 6, *E* and *F*). We found that transduction of dcKO BMMs with MFN2-AA restored osteoclastogenesis to a level comparable with MFN2-WT, indicating that the mitophagy function of MFN2 is dispensable for osteoclastogenesis. In contrast, transduction with MFN2-EE had only a minimal effect on osteoclastogenesis, suggesting that tethering/fusion by MFN2 is necessary for osteoclastogenesis to occur efficiently (Fig. 6, *C–F*). Because MNF1 was absent from these cells, this reveals that mitochondrial tethering by MFN2 contributes to OC formation in a way that MFN1 cannot.

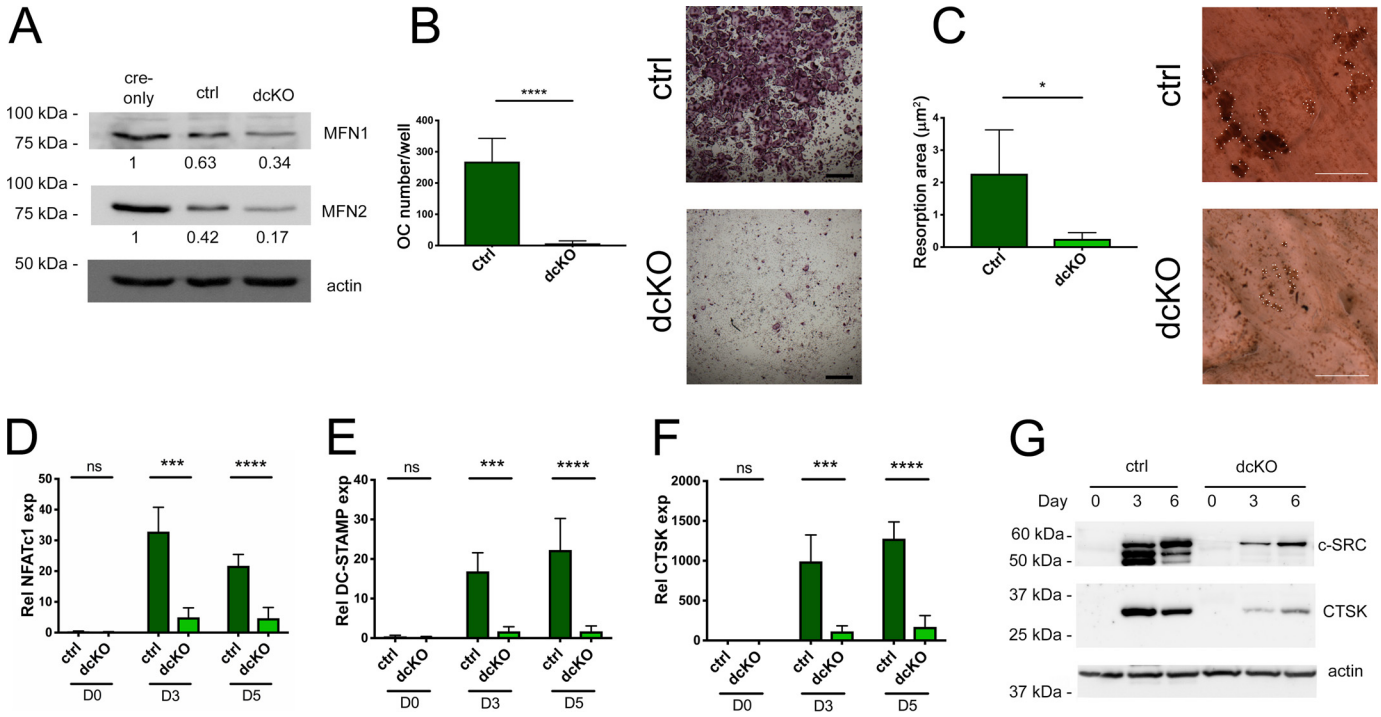

Figure 3. Osteoclastogenesis is defective in BMMs derived from dcKO bone marrow. *A*, MFN1 and MFN2 protein levels are progressively decreased in RANKL-treated ctrls and dcKOs compared with RANKL-treated cre-only BMMs. *B*, BMMs cultured with RANKL for 5 days form OCs in ctrls but not in dcKOs. *Scale bars* = 400 μm. *C*, bone resorption is congruently inhibited; resorption pits are outlined in *dotted white*. *Scale bars* = 200 μm. *D–G*, mRNA levels of the OC markers NFATc1 (*D*), DC-STAMP (*E*), and CTSK (*F*) are diminished in dcKOs after 3 and 5 days of differentiation in RANKL, correlating with C-SRC and CTSK protein levels during osteoclastogenesis (*G*). *, $p < 0.05$; ***, $p < 0.001$; ****, $p < 0.0001$; *ns*, not significant; unpaired *t* test with Welch's correction. $n = 3$ biological replicates.

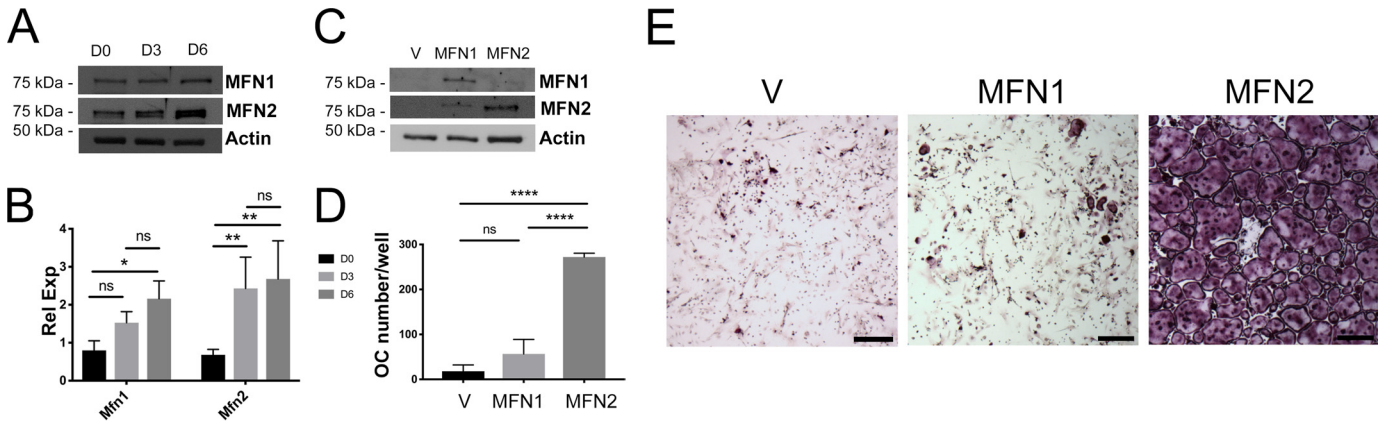

Figure 4. Although both homologs increase during OC formation, addition of MFN2 drives osteoclastogenesis *in vitro* more efficiently. *A* and *B*, protein (*A*) and mRNA (*B*) expression through 6 days of osteoclastogenesis in WT BMMs shows parallel increases in MFN1 and MFN2 expression. *C*, dcKO BMMs were transduced with retroviral pMX-Vector, V, pMX-MFN1, MFN1, or pMX-MFN2, and mitofusin proteins were detected via Western blotting. *D* and *E*, following RANKL treatment for 6 days, cultures were stained with TRAP, and OCs were enumerated, revealing robust osteoclastogenesis in MFN2-treated but not MFN1-treated cells. The graphs represent three biological replicates. *Scale bars* = 400 μm. *, $p < 0.05$; **, $p < 0.01$; ****, $p < 0.0001$; *ns*, not significant; one-way ANOVA.

Ca^{2+} signaling is perturbed in pre-OCs with impaired MFN2-mediated tethering

To further explore the mechanism through which MFN2 controls osteoclastogenesis, we assayed cytoplasmic Ca^{2+} levels with Fura-2 basally, following ATP stimulation (to release ER calcium stores) and after addition of extracellular calcium (2 mM) to activate store-operated calcium entry (SOCE). In pre-OCs generated with 48 h of RANKL exposure, dcKOs had higher basal Ca^{2+} levels and a similar ATP-mediated spike from baseline but a muted intake of Ca^{2+} following SOCE activation compared with ctrls, as assessed by area under curve quantification (Fig. 7, *A–C*). We used the same assay in dcKO BMMs overexpressing MFN2-WT, -EE, and -AA. Compared with the vector control, MFN2-WT and MFN2-AA increased responsiveness to extracellular Ca^{2+} whereas MFN2-EE did not, suggesting that the tethering function of MFN2 regulates SOCE (Fig. 7, *D–F*). Congruent with restoration of osteoclastogenesis, cells with improved SOCE (MFN2-WT and -AA) had increased NFATc1 levels compared with dcKOs with V or MFN2-EE transduction,

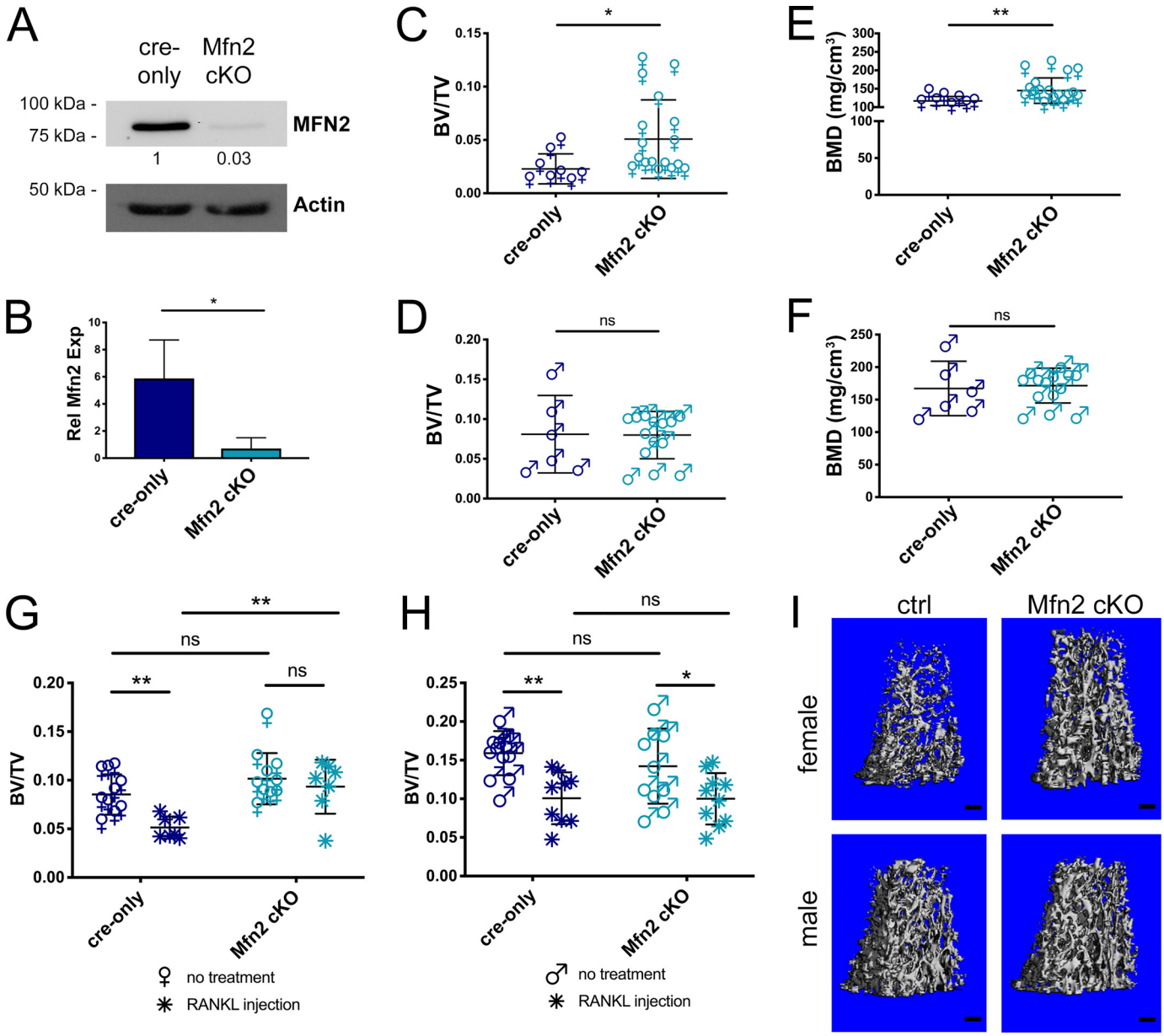

Figure 5. Female mice lacking MFN2 alone in the OC lineage are protected from bone loss with age and RANKL-induced osteolysis. *A* and *B*, MFN2 expression is decreased in Mfn2 cKO OCs *in vitro* compared with cre-only at the protein (*A*) and RNA (*B*) levels. *C–F*, femora from cre-only and Mfn2 cKO mice at 12 months of age were analyzed by μCT for BV/TV in females (*C*), BV/TV in males (*D*), BMD in females (*E*), and BMD in males (*F*). Trabecular bone mass is increased in female cKOs but not males. *G–I*, acute bone loss was induced by intraperitoneal RANKL injection at 2 months of age in cre-only and Mfn2 cKO mice, and assessed by μCT at the distal femur. BV/TV is not decreased with RANKL treatment in female Mfn2 cKO mice (*G*). BV/TV decreases to a similar degree in male Mfn2 cKO mice compared with cre-only controls (*H*). *I*, representative post-RANKL μCT reconstructions from *G* and *H*. *Scale bars* = 200 μm. The untreated cohorts are the same as those listed at 2 months of age in Table 1 and Table S1. *, $p < 0.05$; **, $p < 0.01$; *ns*, not significant; unpaired *t* test with Welch's correction in *B–F* and ordinary two-way ANOVA with multiple comparisons in *G* and *H*.

linking the MFN2 tethering function to the Ca^{2+}–NFATc1 axis during OC differentiation (Fig. 7*G*).

Discussion

An abundance of mitochondria has been deemed important for function of the OC, and increases in mitochondrial proteins are associated with differentiation from myeloid precursors (16, 26, 27). Mitochondrial biogenesis, mediated by PGC1α and PGC1β, plays an important role, as global deletion of either of these factors leads to increased trabecular bone mass (17, 28). Further, conditional PGC1β deletion in OCs results in impaired cytoskeletal organization and bone resorption (19). OCs have been reported to utilize oxidative phosphorylation and aerobic glycolysis, and it has been suggested that the primary function of mitochondria may not be ATP generation at the ruffled border (29).

To better understand the role of mitochondria and put into context the elongated organelles observed in human OCs (27), we aimed to perturb mitochondrial network organization. We found that dual depletion of the key mitochondrial dynamics proteins MFN1 and MFN2 in the OC lineage leads to increased bone mass in female mice *in vivo*, accom-

Table 1
Trabecular bone parameters are increased in female Mfn2 cKOs at 12 months of age
Femora from female cre-only and Mfn2 cKO mice were analyzed by μCT at 2, 4, and 12 months (mo.) of age, revealing high bone mass in Mfn2 cKOs at 1 year. *, $p < 0.05$; **, $p < 0.01$; unpaired t-test with Welch's correction.

		Female cre-only	Female Mfn2 cKO	*p* value
BV/TV	2 mo.	0.085 ± 0.021	0.102 ± 0.026	0.145
	4 mo.	0.096 ± 0.014	0.111 ± 0.032	0.175
	12 mo.	0.023 ± 0.014	0.051 ± 0.037	0.012*
BMD (mg/cm^3)	2 mo.	180.9 ± 18.3	195.4 ± 20.6	0.115
	4 mo.	193.5 ± 12.4	205.3 ± 23.5	0.166
	12 mo.	116.9 ± 12.2	145 ± 34.5	0.007**
Tb.N. (no./mm)	2 mo.	4.20 ± 0.34	4.53 ± 0.45	0.099
	4 mo.	3.53 ± 0.22	3.81 ± 0.30	0.027*
	12 mo.	1.78 ± 0.53	2.15 ± 0.39	0.103
Tb.Th. (mm)	2 mo.	0.040 ± 0.003	0.041 ± 0.003	0.295
	4 mo.	0.044 ± 0.002	0.046 ± 0.004	0.288
	12 mo.	0.051 ± 0.006	0.050 ± 0.006	0.495
Tb.Sp. (mm)	2 mo.	0.239 ± 0.024	0.220 ± 0.023	0.082
	4 mo.	0.284 ± 0.018	0.262 ± 0.023	0.022*
	12 mo.	0.605 ± 0.150	0.481 ± 0.083	0.057
Cort.Th. (mm)	2 mo.	0.145 ± 0.014	0.159 ± 0.011	0.023*
	4 mo.	0.204 ± 0.017	0.207 ± 0.014	0.752
	12 mo.	0.201 ± 0.028	0.226 ± 0.007	0.055

panied by a decrease in serum CTX-1 levels. This corresponds to an inability of OCs derived from these dcKO animals to form in culture. Previous work in the field has focused primarily on how changes in mitochondrial content and oxidative phosphorylation impact OC resorption (16, 19, 30, 31). Our model expands the relationship between mitochondria and OCs by linking disruption of mitochondrial dynamics to inhibition of OC formation.

To determine whether MFN1 and MFN2 contribute differentially to OC formation, we overexpressed each homolog in dcKO BMMs in culture and found that osteoclastogenesis was much more efficient with MFN2 than MFN1 addition. Further, loss of MFN2 alone led to increased bone mass *in vivo*, albeit delayed compared with the doubly deficient cohort. Similarly, work with heart and skeletal muscle has revealed that loss of MFN1 and MFN2 produces more severe phenotypes than single knockout of either mitofusin (14, 32). It is likely that the mitochondrial fusion function of MFN2 plays some role in OCs, which allows compensation by MFN1 to reduce the severity of bone accrual in MFN2 singly deficient mice, although at least one MFN2-unique role is also important.

MFN2, but not MFN1, functions in mitophagy, mitochondrial transport in axons, and ER–mitochondrion interactions. Phenotypic effects of specific mutations reveal significant cell type specificity in these various roles. For example, fibroblasts derived from CMT2A patients show differences in ER–mitochondrion spacing that correlate with disease severity, suggesting that alteration of ER–mitochondrion tethering contributes to pathogenicity in humans (33). In contrast, mitophagy is required for metabolic reprogramming of mammalian hearts during perinatal development, but tethering by MFN2 is dispensable for this process (24). We utilized point mutants separating tethering and mitophagy functions to probe which MFN2 function is important in the OC lineage and found that the tethering function of MFN2 is necessary for osteoclastogenesis.

The master OC transcription factor NFATc1 depends on cytoplasmic Ca^{2+} flux and requires dephosphorylation by calcineurin for translocation to the nucleus (34), leading to amplification because of binding at its own promoter. We find that NFATc1 mRNA levels are diminished in our dcKO cells, suggesting alterations in Ca^{2+} handling. The ER–mitochondrion juxtaposition, regulated by the tethering function of MFN2 but not MFN1, is known to impact Ca^{2+} signaling (9, 33, 35). We therefore examined cytoplasmic Ca^{2+} levels and found that dcKOs had a significantly reduced magnitude of SOCE. Similar blunting of SOCE was found in C2C12 myoblasts with MFN2 knockdown (36). Interestingly, our dcKOs showed higher basal cytoplasmic Ca^{2+}, whereas MFN2-depleted C2C12 cells and BMMs had lower basal cytoplasmic Ca^{2+} than controls (36, 37). It is possible that the presence of MFN1 in the experiments with MFN2 knockdown plays a role in basal levels, whereas MFN2 is more important for SOCE regulation. On our MFN1/MFN2-deficient background, we further found that the tethering-competent/mitophagy-deficient MFN2-AA, but not the tethering-deficient/mitophagy-activated MFN2-EE, restored SOCE along with NFATc1 induction and osteoclastogenesis. Previously, we found that cells lacking TMEM178, which show increased NFATc1 and osteoclastogenesis, have elevations in basal cytoplasmic Ca^{2+} and SOCE (38, 39). Thus, it is likely that the magnitude of Ca^{2+} excursions, rather than the basal level, is more important for osteoclastogenesis. Mechanistically, we propose that MFN2-mediated restoration of ER-mitochondrion contacts, which regulate mitochondrial Ca^{2+} uptake, are responsible for the ability of cells to generate the large swings in cytoplasmic Ca^{2+} (*i.e.* high-amplitude oscillations) that drive NFATc1 activation.

We find striking sexual differences in our bone phenotypes, and to our knowledge, this is the second report of differential male *versus* female responses to mitofusin loss. Conditional ablation of MFN2 in brown adipose tissue leads to sex-specific remodeling of mitochondrial function; females displayed increased ATP-synthesizing fatty acid oxidation, whereas males experienced increased glycolytic capacity (40, 41). Although loss of MFN2 in brown adipose tissue caused distinct abnormalities in males and females, we only saw changes in females with loss of mitofusins in the OC lineage. We previously found higher OC numbers in the trabecular compartment of female mice, possibly explaining the greater impact on bone mass with more abundant OCs in this sex (42). One explanation could be that there is a threshold effect for mitofusins on OC formation and that females are more sensitive to mitofusin depletion than males. Further, the high bone mass phenotype may be more severe in female dcKOs compared with single Mfn2 cKOs because residual MFN1 expression partially compensates for loss of MFN2. Consistent with this threshold hypothesis, we see no differences in bone mass between cre-only and double heterozygous ctrl animals despite protein levels differing by about half. Because residual mitofusin proteins were detected in our lysM-cre models, greater effects, including increased bone mass in male mice, might be achieved with more complete recombination in the OC lineage. Future investigations can utilize RANK-cre to target a similar early devel-

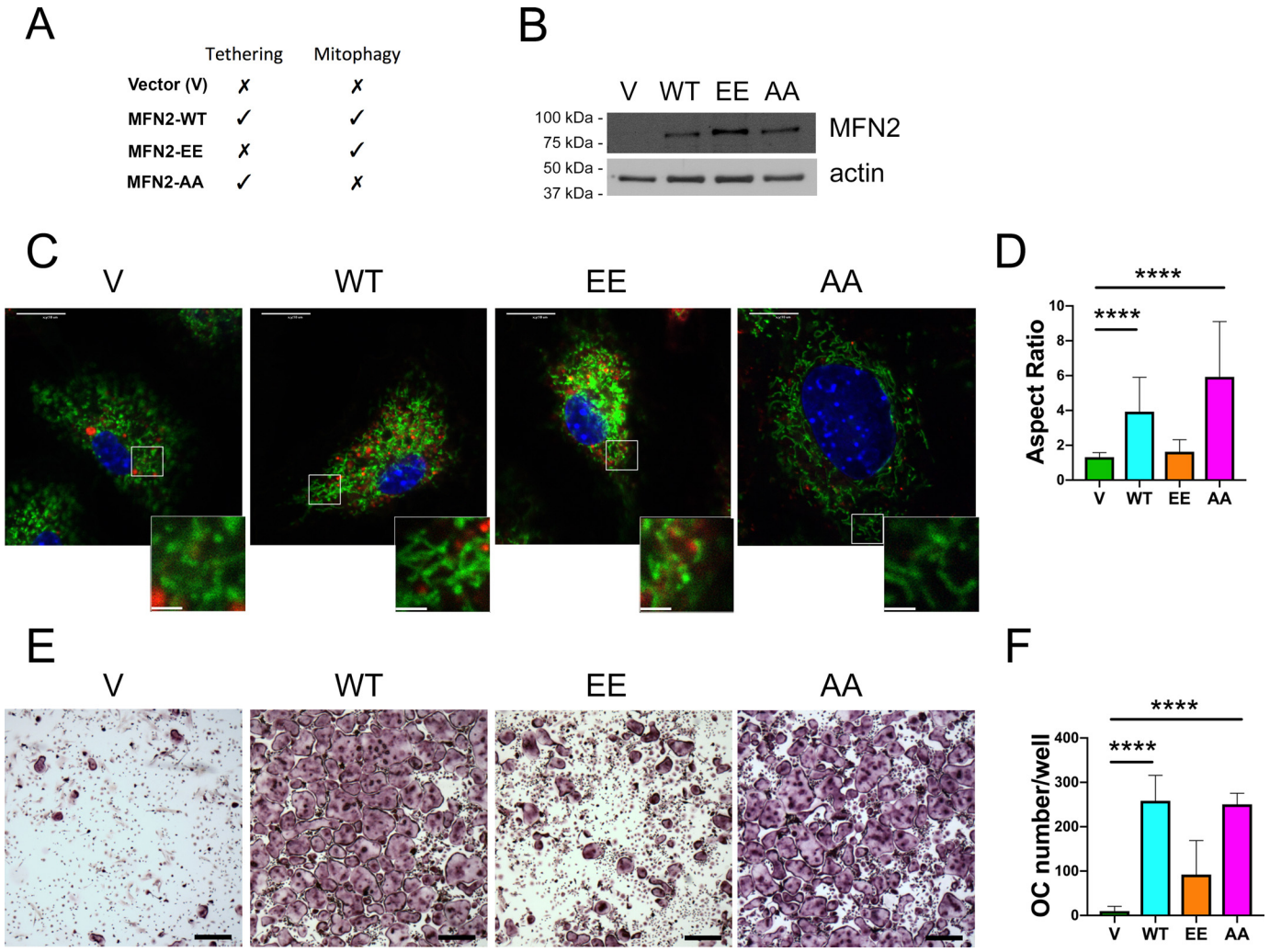

Figure 6. Restoration of MFN2 tethering function rescues osteoclastogenesis in dcKO BMMs. *A*, MFN2 functions in each rescue condition. *B*, dcKO BMMs were transduced with retroviral pMX-Vector (*V*), pMX-MFN2-WT (*WT*), pMX-MFN2-EE (*EE*), and pMX-MFN2-AA (*AA*), and MFN2 protein was detected via Western blotting in BMMs. *C*, cultures of transduced BMMs were stained with MitoTracker Green and LysoTracker Red. *Scale bars* = 10 μm (*whole cells*) and 2.5 μm (*insets*). *D*, quantification of mitochondrial aspect ratio (mitochondrial length/width). *E*, BMMs were TRAP-stained following 6 days of RANKL exposure, revealing robust osteoclastogenesis with MFN2-AA but not MFN2-EE. *Scale bars* = 400 μm. *F*, quantification of OC numbers in three biological replicates. ****, $p < 0.0001$, ordinary one-way ANOVA.

opmental stage or Cathepsin K–cre to deplete mitofusins in mature OCs.

In sum, our studies highlight the importance of mitofusin-mediated organelle tethering in OC lineage cells and suggest that mitochondrial dynamics are important in control of bone resorption, at least in females. Preclinical experiments have suggested that down-regulation of MFN2 may have beneficial effects in cardiac ischemia (43, 44), and our work opens the possibility that it may also preserve bone mass in women.

Experimental procedures

Mice

Double floxed *Mfn1*$^{fl/fl}$; *Mfn1/2*$^{fl/fl}$ animals (45), which delete exon 4 of *MFN1* and exon 6 of *MFN2* upon cre recombination, were mated to C57Bl/6 mice harboring the LysozymeM-cre recombinase (LysM-cre) allele (46) to place all animals on a homozygous LysM-cre background. To generate dcKOs, double heterozygous (*Mfn1*$^{fl/+}$; *Mfn2*$^{fl/+}$;*LysM*$^{c/c}$) mice were first bred together, and dcKO (*Mfn1*$^{fl/fl}$; *Mfn1/2*$^{fl/fl}$; *LysM*$^{c/c}$) female progeny were mated to double-heterozygous males to generate the cohort of double heterozygous controls and dcKOs. In parallel, cre-only (*Mfn1*$^{+/+}$; *Mfn2*$^{+/+}$; *LysM*$^{c/c}$) females from the original double-heterozygous matings were bred to double-heterozygous males to generate the cohort of cre-only and control animals. The single Mfn2 cohort was generated using heterozygous breeding pairs so that progeny genotypes included cre-only (*Mfn2*$^{+/+}$; *LysM*$^{c/c}$) and cKOs (*Mfn1/2*$^{fl/fl}$; *LysM*$^{c/c}$).

Mice were housed communally with *ad libitum* access to fresh chow and water in a pathogen-free, temperature-controlled barrier facility. Daily observation and weekly cage changes were provided by staff of the Division of Comparative Medicine. Laboratory members coordinated animal husbandry and breeding, and the Division of Comparative Medicine veterinarian assessed all health concerns. All protocols were approved by Washington University School of Medicine's Animal Studies Committee (protocol 20170025).

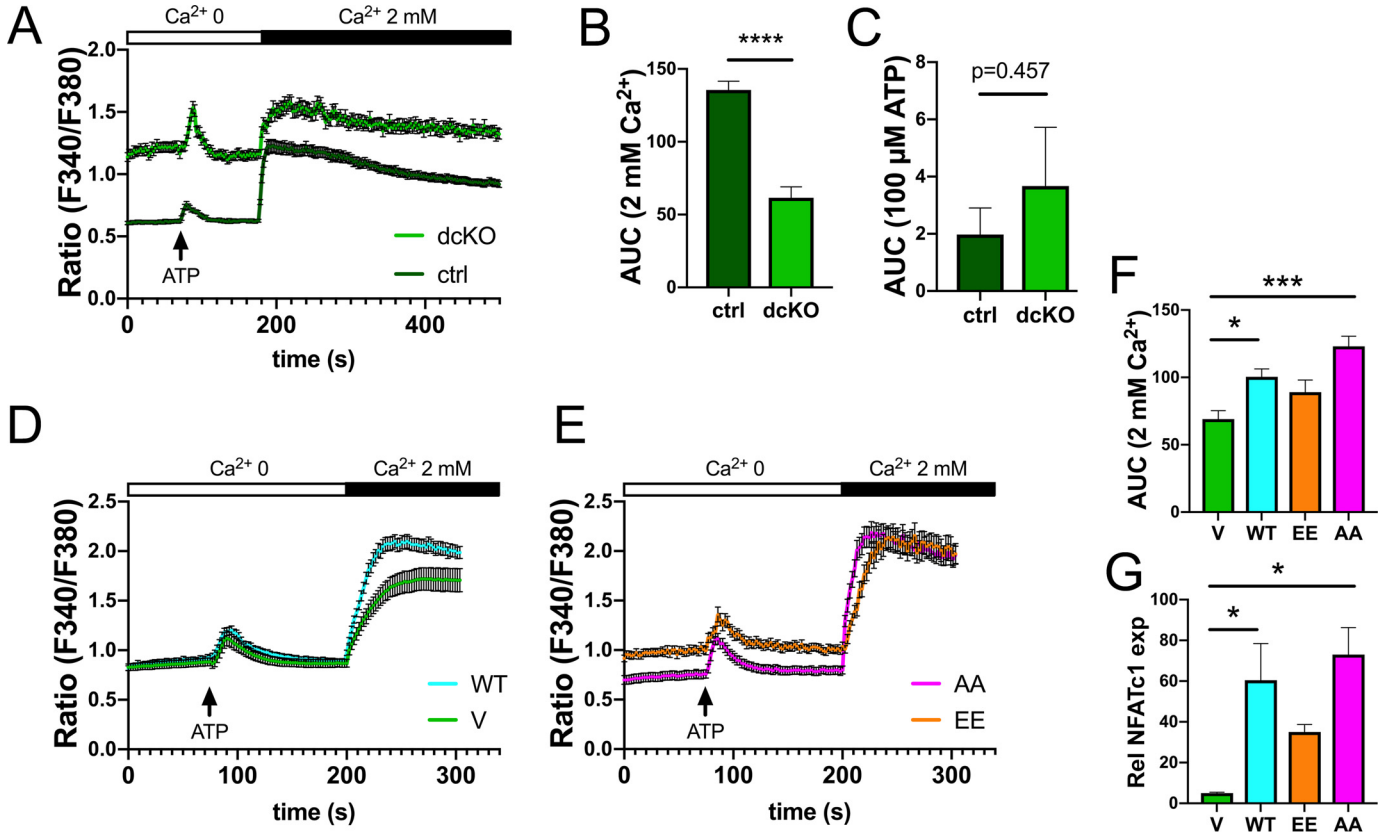

Figure 7. Blunted Ca^{2+} entry in dcKO preOCs is restored with MFN2-AA overexpression. *A–C*, Fura-2 staining shows elevated basal intracellular Ca^{2+} but blunted store-operated calcium entry after addition of extracellular Ca^{2+} in dcKO pre-OCs. Shown is area under the curve quantification following Ca^{2+} (*B*) and ATP (*C*). *D* and *E*, overexpression of MFN2-WT or MFN2-AA restores Ca^{2+} entry in dcKO pre-OCs whereas MFN2-EE does not. *F*, quantification of the area under the curve. *G*, corresponding NFATc1 levels, evaluated by quantitative real-time PCR in mutant OCs, correlate with SOCE responsiveness. *, $p < 0.05$; ***, $p < 0.001$; ****, $p < 0.0001$; unpaired *t* test (*B* and *C*) or ordinary one-way ANOVA (*F* and *G*).

Micro-computed tomography

Following dissection of right femora from 2-, 4-, and 12-month-old animals, bones were fixed in 10% neutral buffered formalin (Di Ruscio & Associates, Inc., Fenton, MO) for 24 h and then stored in 70% ethanol. Trabecular and cortical scans were acquired proximal to the distal growth plate and at the mid-shaft of femora, respectively (μCT40, Scanco, Brüttisellen, Switzerland; 10-μm resolution, 55 kilovoltage peak, 145 μA, 300-s integration time). Thresholds were determined in a blinded manner and analyzed with reference to accepted guidelines (47, 48).

CTX1 and P1NP

Serum was collected from animals fasted overnight via mandibular bleed (BD Microtainer) and stored at −80 °C. RatLaps CTX-1 and P1NP EIA assays were conducted according to manufacturer's instructions (Immunodiagnostic Systems, Gaithersburg, MD; AC-06F1 and AC-33F1, respectively).

Histomorphometry

2-month-old mice were injected i.p. with 10 mg/kg calcein (C0875, Sigma) and 30 mg/kg Alizarin Red (A3882, Sigma) 7 and 2 days prior to sacrifice, respectively. Intact femora/tibiae were fixed in 10% neutral buffered formalin for 24 h prior to storage in 70% ethanol. Tissues were embedded in methylmethacrylate and sectioned sagittally by the Washington University Musculoskeletal Histology and Morphometry Core. Unstained and TRAP-stained (Sigma) slides were imaged at ×20 high resolution using a NanoZoomer 2.0 with bright field and FITC/TRITC (Hamamatsu Photonics). Images were then analyzed via Bioquant Osteo software according to the manufacturer's instructions and published standards (v18.2.6, Bioquant Image Analysis Corp., Nashville, TN) (49).

BMM isolation and osteoclast differentiation

BMMs were harvested by collecting bone marrow from dissected long bones of 2-month-old female animals via centrifugation at 10,000 rpm, passed through a 40-μm filter, and cultured with α-MEM (Sigma, M0894) containing 10% FBS (Gibco), 100 IU/ml penicillin/streptomycin, and 1:10 dilution of CMG 14-12 cell supernatant containing an equivalent of 100 ng/ml Macrophage-Colony Stimulating Factor (M-CSF) (20, 50).

Expanded BMMs were plated at a density of 9,000 and 300,000 cells/well for 96- and 6-well plates, respectively. Purified GST-RANKL at 30 ng/ml was added to α-MEM containing 10% FBS, 100 IU/ml penicillin/streptomycin, and a 1:50 dilution of CMG 14-12 cell supernatant. The medium was changed every alternate day until control wells were filled with multinucleated OCs. TRAP stains were employed following 10-min fix-

ation with 4% paraformaldehyde (Polysciences, Warrington, PA) and 0.1% Triton X-100 in PBS according to the manufacturer's instructions (Sigma, 387A).

Resorption assay

Expanded BMMs were seeded on bovine bone slices and differentiated to OCs with purified GST-RANKL as above. At maturity, bone slices were fixed for 10 min with 4% paraformaldehyde and 0.1% Triton X-100 in PBS. Bone slices were incubated in 0.5 NaOH for 30 s and kept hydrated in PBS. Cells were scraped off bone slices with a cotton swab, and bone slices were incubated with 20 μg/ml peroxidase-conjugated wheat germ agglutinin in PBS (Sigma, 61767) for 30 min. Subsequently, slices were washed three times in PBS and incubated with a DAB Chromogen Kit (Biocare Medical, BDB2004H) at 37 °C for 30 min. Slices were left to air-dry and imaged under a bright field at ×20.

Quantitative real-time PCR

Following collection of cells with TRIzol (Life Technologies), solutions were centrifuged at 12,000 × *g*, and the aqueous layer was extracted with phenol:chloroform. An equal volume of 70% ethanol was added, and the remaining RNA isolation was done using the NucleoSpin RNA II Kit (Clontech Laboratories, Palo Alto, CA; 740955.50). 1 μg of RNA was placed into the cDNA Ecodry Premix Kit prior to the quantitative PCR program being run on ABI QuantStudio 3 with iTaq Universal SYBR Green Supermix (Bio-Rad, 1725121). Each reaction proceeded at 50 °C for 2 min, 95 °C for 10 min, and then 40 cycles of 95 °C for 15 s and 60 °C for 1 min. Relative expression was calculated as $100 \times 2^{-\text{(target CT} - \text{B2M CT)}}$. Primer sequences were as follows: MFN1, TTGGCAGGACAAGTAGTGGC (forward) and AGCAGTTGGTTGTGTGACCA (reverse); MFN2, AAGCACTTTGTCACTGCCAAG (forward) and TTGTCCCAGAGCATGGCATTG (reverse); NFATc1, GGTAACTCTGTCTTTCTAACCTTAAGCTC (forward) and GTGATGACCCCAGCATGCACCAGTCACA (reverse); DC-STAMP, ACAAACAGTTCCAAAGCTTGC (forward) and TCCTTGGGTTCCTTGCTTC (reverse); CTSK, AGGCAGCTAAATGCAGAGGGTACA (forward) and AGCTTGCATCGATGGACACAGAGA (reverse); B2M, CTGCTACGTAACACAGTTCCACCC (forward) and CATGATGCTTGATCACATGTCTCG (reverse).

Western blotting

Radioimmune precipitation assay buffer (20 mM Tris (pH 7.5), 150 mM NaCl, 1 mM EDTA, 1 mM EGTA, 1% Triton X-100, 2.5 mM sodium pyrophosphate, 1 mM β-glycerophosphate, 1 mM Na_3VO_4, and 1 mM NaF) with 1:50 HALT protease and phosphatase inhibitor (Thermo Fisher Scientific, Waltham, MA; 1861280) was used to lyse BMM and OC cells following two washes in PBS. Lysates were vortexed and centrifuged at 700 × *g*. Supernatant was quantified with a BCA assay (Bio-Rad), and 20 μg was loaded to a 10% SDS-PAGE gel. Gels were run at 80 V for 2 h and transferred to nitrocellulose by wet transfer at 100 V for 90 min. Blocking was done in TBS and 0.1% Tween 20 with 5% milk. Membranes were probed with primary antibodies overnight at 4 °C (sc-50330, 1:500, Mfn1, Santa Cruz Biotechnology, Dallas, TX; ab56889, 1:1000, Mfn2, Abcam, Cambridge, UK; MAB3324, 1:1000, CTSK, EMD Millipore, Burlington, MA; and c-Src, 1:1000, a mAB developed by S. Teitelbaum, St. Louis, MO). Actin was used as a loading control at 1:10,000 (A228, Sigma-Aldrich, St. Louis, MO). Imaging was done using SuperSignal West Femto substrate (Thermo Fisher Scientific, 34095) and a chemiluminescence imager (Syngene, Cambridge, UK).

Retroviral overexpression

MFN1-Myc and MFN2-Myc were obtained from Addgene (plasmids 23212 and 23213, respectively). MFN2-WT, MFN2-EE, and MFN2-AA were generated by Gerald Dorn (24). Each gene was cloned into the pMX retroviral vector and transfected into Platinum-E (platE) cells by calcium phosphate precipitation (51, 52). Each insert was also sequenced to verify the presence or absence of the desired point mutations. PlatE supernatant was harvested 48 and 72 h post-transfection, filtered through 0.45 μm, and added to BMMs with α-MEM, 10% FBS, and 100 IU/ml penicillin/streptomycin, 1:10 CMG, and 8 μg/ml Polybrene (Sigma, H9268) on 2 consecutive days. 24 h following final virus addition, 1 μg/ml blasticidin (Sigma, 203350) was added to select infected BMMs.

Induced osteolysis

2 month old ctrl and Mfn2 cKO animals were injected i.p. with 1 mg/kg of body weight GST-RANKL twice, 24 h apart, as published previously (53). 50 h after the first injection, animals were sacrificed, and femoral trabecular bone was evaluated by μCT.

Confocal imaging

Cultured BMMs transduced with vector, MFN2-WT, MFN2-EE, and MFN2-AA retroviruses were plated on 25-mm glass round coverslips at 500,000 cells/well, washed with phenol red-free DMEM (Thermo Fisher), and stained with 200 nM MitoTracker Green FM and 200 nM LysoTracker Red (M7514 and L7528, Molecular Probes, Eugene, OR) for 30 min at 37 °C. Following incubation, cells were washed again and kept in DMEM with 10% FBS, 10% CMG, and 10 μg/ml Hoechst (Thermo Fisher). Confocal imaging was performed on a Nikon Ti confocal microscope using a ×60 1.3 numerical aperture oil immersion objective with the coverglass loaded onto a chamber (Warner Instruments, RC-40LP, Hamden, CT) in modified Krebs–Henseleit buffer (138 mM NaCl, 3.7 mM KCl, 1.2 mM KH_2PO_4, 15 mM glucose, 20 mM HEPES, and 1 mM $CaCl_2$).

Cytoplasmic Ca^{2+} measurement

BMMs were plated in 29-mm glass-bottom plates at 300,000 cells/plate (Cellvis, D29-14-1.5-N, Mountain View, CA) and exposed to 30 ng/ml RANKL for 48 h. Cells were washed and incubated at 37° for 30 min in Hanks' balanced salt solution (HBSS) containing 2 mM $CaCl_2$, 1 mM $MgCl_2$, 10 ng/ml humanM-CSF (Biolegend), 30 ng/ml RANKL, and 2 μM Fura-2. Cells were washed and kept in Hanks' balanced salt solution with 1 mM $MgCl_2$ without Ca^{2+}, 10 ng/ml humanM-CSF, and 30 ng/ml RANKL for imaging. 35–85 cells/plate were measured at wavelengths of 340 and 380 every 2 s on an Olympus IX-71 inverted microscope with a Lamda-LS illuminator at the

Washington University Hope Center and the Center for Investigation of Membrane Excitability Diseases Live Cell Imaging Facility. 100 μM ATP and 2 mM $CaCl_2$ were used as stimuli as indicated.

Statistics

Two-way ANOVA with Tukey's multiple comparisons and one- or two-tailed unpaired *t* tests with Welch's correction were performed with GraphPad Prism built-in statistical analysis (GraphPad Software, Inc., La Jolla, CA). All data are represented as mean ± S.D. with three or more biological replicates. *p* values are designated as follows: *, $p < 0.05$; **, $p < 0.01$; ***, $p < 0.001$; ****, $p < 0.0001$.

Data availability

All data are contained within the manuscript.

Author contributions—A. B., R. Z., A. Z., C. S., L. C., H. Y., and A. F. data curation; A. B., R. Z., and C. S. formal analysis; A. B. and R. Z. validation; A. B. and D. J. V. writing-original draft; A. B., R. F., and D. J. V. writing-review and editing; R. Z. methodology; A. Z., L. C., H. Y., and A. F. investigation; H. Y. and A. F. visualization; G. W. D., R. F., and D. J. V. conceptualization; G. W. D. and R. F. supervision.

Acknowledgments—We thank Crystal Idleburg, Samantha Coleman, and Michael Brodt for technical assistance.

References

1. Schrepfer, E., and Scorrano, L. (2016) Mitofusins, from mitochondria to metabolism. *Mol. Cell* **61,** 683–694 CrossRef Medline
2. Dorn, G. W., 2nd, Vega, R. B., and Kelly, D. P. (2015) Mitochondrial biogenesis and dynamics in the developing and diseased heart. *Genes Dev.* **29,** 1981–1991 CrossRef Medline
3. Chen, H., Detmer, S. A., Ewald, A. J., Griffin, E. E., Fraser, S. E., and Chan, D. C. (2003) Mitofusins Mfn1 and Mfn2 coordinately regulate mitochondrial fusion and are essential for embryonic development. *J. Cell Biol.* **160,** 189–200 CrossRef Medline
4. Filadi, R., Pendin, D., and Pizzo, P. (2018) Mitofusin 2: from functions to disease. *Cell Death Dis.* **9,** 330–343 CrossRef Medline
5. Celsi, F., Pizzo, P., Brini, M., Leo, S., Fotino, C., Pinton, P., and Rizzuto, R. (2009) Mitochondria, calcium and cell death: a deadly triad in neurodegeneration. *Biochim. Biophys. Acta* **1787,** 335–344 CrossRef Medline
6. Züchner, S., Mersiyanova, I. V., Muglia, M., Bissar-Tadmouri, N., Rochelle, J., Dadali, E. L., Zappia, M., Nelis, E., Patitucci, A., Senderek, J., Parman, Y., Evgrafov, O., Jonghe, P. D., Takahashi, Y., Tsuji, S., *et al.* (2004) Mutations in the mitochondrial GTPase mitofusin 2 cause Charcot-Marie-Tooth neuropathy type 2A. *Nat. Genet.* **36,** 449–451 CrossRef Medline
7. Strickland, A. V., Rebelo, A. P., Zhang, F., Price, J., Bolon, B., Silva, J. P., Wen, R., and Züchner, S. (2014) Characterization of the mitofusin 2 R94W mutation in a knock-in mouse model. *J. Peripher. Nerv. Syst.* **19,** 152–164 CrossRef Medline
8. Zhou, Y., Carmona, S., Muhammad, A. K. M. G., Bell, S., Landeros, J., Vazquez, M., Ho, R., Franco, A., Lu, B., Dorn, G. W., 2nd, Wang, S., Lutz, C. M., and Baloh, R. H. (2019) Restoring mitofusin balance prevents axonal degeneration in a Charcot-Marie-Tooth type 2A model. *J. Clin. Invest.* **130,** 1756–1771 Medline
9. Bernard-Marissal, N., van Hameren, G., Juneja, M., Pellegrino, C., Louhivuori, L., Bartesaghi, L., Rochat, C., El Mansour, O., Médard, J.-J., Croisier, M., Maclachlan, C., Poirot, O., Uhlén, P., Timmerman, V., Tricaud, N., *et al.* (2019) Altered interplay between endoplasmic reticulum and mitochondria in Charcot-Marie-Tooth type 2A neuropathy. *Proc. Natl. Acad. Sci. U.S.A.* **116,** 2328–2337 CrossRef Medline
10. Saporta, M. A., Dang, V., Volfson, D., Zou, B., Xie, X. S., Adebola, A., Liem, R. K., Shy, M., and Dimos, J. T. (2015) Axonal Charcot-Marie-Tooth disease patient-derived motor neurons demonstrate disease-specific phenotypes including abnormal electrophysiological properties. *Exp. Neurol.* **263,** 190–199 CrossRef Medline
11. Loiseau, D., Chevrollier, A., Verny, C., Guillet, V., Gueguen, N., Pou de Crescenzo, M.-A., Ferré, M., Malinge, M.-C., Guichet, A., Nicolas, G., Amati-Bonneau, P., Malthièry, Y., Bonneau, D., and Reynier, P. (2007) Mitochondrial coupling defect in Charcot-Marie-Tooth type 2A disease. *Ann. Neurol.* **61,** 315–323 CrossRef Medline
12. Eschenbacher, W. H., Song, M., Chen, Y., Bhandari, P., Zhao, P., Jowdy, C. C., Engelhard, J. T., and Dorn, G. W., 2nd (2012) Two rare human mitofusin 2 mutations alter mitochondrial dynamics and induce retinal and cardiac pathology in *Drosophila*. *PLoS ONE* **7,** e44296 CrossRef Medline
13. Guo, X., Chen, K.-H., Guo, Y., Liao, H., Tang, J., and Xiao, R.-P. (2007) Mitofusin 2 triggers vascular smooth muscle cell apoptosis via mitochondrial death pathway. *Circ. Res.* **101,** 1113–1122 CrossRef Medline
14. Chen, H., Vermulst, M., Wang, Y. E., Chomyn, A., Prolla, T. A., McCaffery, J. M., and Chan, D. C. (2010) Mitochondrial fusion is required for mtDNA stability in skeletal muscle and tolerance of mtDNA mutations. *Cell* **141,** 280–289 CrossRef Medline
15. Sebastián, D., Sorianello, E., Segalés, J., Irazoki, A., Ruiz-Bonilla, V., Sala, D., Planet, E., Berenguer-Llergo, A., Muñoz, J. P., Sánchez-Feutrie, M., Plana, N., Hernández-Álvarez, M. I., Serrano, A. L., Palacín, M., and Zorzano, A. (2016) Mfn2 deficiency links age-related sarcopenia and impaired autophagy to activation of an adaptive mitophagy pathway. *EMBO J.* **35,** 1677–1693 CrossRef Medline
16. Zeng, R., Faccio, R., and Novack, D. V. (2015) Alternative NF-κB regulates RANKL-induced osteoclast differentiation and mitochondrial biogenesis via independent mechanisms. *J. Bone Miner. Res.* **30,** 2287–2299 CrossRef Medline
17. Ishii, K.-A., Fumoto, T., Iwai, K., Takeshita, S., Ito, M., Shimohata, N., Aburatani, H., Taketani, S., Lelliott, C. J., Vidal-Puig, A., and Ikeda, K. (2009) Coordination of PGC-1β and iron uptake in mitochondrial biogenesis and osteoclast activation. *Nat. Med.* **15,** 259–266 CrossRef Medline
18. Wei, W., Wang, X., Yang, M., Smith, L. C., Dechow, P. C., Sonoda, J., Evans, R. M., and Wan, Y. (2010) PGC1β mediates PPARγ activation of osteoclastogenesis and rosiglitazone-induced bone loss. *Cell Metab.* **11,** 503–516 CrossRef Medline
19. Zhang, Y., Rohatgi, N., Veis, D. J., Schilling, J., Teitelbaum, S. L., and Zou, W. (2018) PGC1β organizes the osteoclast cytoskeleton by mitochondrial biogenesis and activation. *J. Bone Miner. Res.* **33,** 1114–1125 CrossRef Medline
20. Novack, D. V., Yin, L., Hagen-Stapleton, A., Schreiber, R. D., Goeddel, D. V., Ross, F. P., and Teitelbaum, S. L. (2003) The IκB function of NF-κB2 p100 controls stimulated osteoclastogenesis. *J. Exp. Med.* **198,** 771–781 CrossRef Medline
21. Vaira, S., Johnson, T., Hirbe, A. C., Alhawagri, M., Anwisye, I., Sammut, B., O'Neal, J., Zou, W., Weilbaecher, K. N., Faccio, R., and Novack, D. V. (2008) RelB is the NF-κB subunit downstream of NIK responsible for osteoclast differentiation. *Proc. Natl. Acad. Sci. U.S.A.* **105,** 3897–3902 CrossRef Medline
22. Wu, Y., Torchia, J., Yao, W., Lane, N. E., Lanier, L. L., Nakamura, M. C., and Humphrey, M. B. (2007) Bone microenvironment specific roles of ITAM adapter signaling during bone remodeling induced by acute estrogen-deficiency. *PLoS ONE* **2,** e586 CrossRef Medline
23. Anginot, A., Dacquin, R., Mazzorana, M., and Jurdic, P. (2007) Lymphocytes and the Dap12 adaptor are key regulators of osteoclast activation associated with gonadal failure. *PLoS ONE* **2,** e585 CrossRef Medline
24. Gong, G., Song, M., Csordas, G., Kelly, D. P., Matkovich, S. J., and Dorn, G. W., 2nd (2015) Parkin-mediated mitophagy directs perinatal cardiac metabolic maturation in mice. *Science* **350,** aad2459 CrossRef Medline
25. Song, M., Mihara, K., Chen, Y., Scorrano, L., and Dorn, G. W., 2nd (2015) Mitochondrial fission and fusion factors reciprocally orchestrate mitophagic culling in mouse hearts and cultured fibroblasts. *Cell Metab.* **21,** 273–286 CrossRef Medline

26. An, E., Narayanan, M., Manes, N. P., and Nita-Lazar, A. (2014) Characterization of functional reprogramming during osteoclast development using quantitative proteomics and mRNA profiling. *Mol. Cell Proteomics* **13,** 2687–2704 CrossRef Medline
27. Lemma, S., Sboarina, M., Porporato, P. E., Zini, N., Sonveaux, P., Di Pompo, G., Baldini, N., and Avnet, S. (2016) Energy metabolism in osteoclast formation and activity. *Int. J. Biochem. Cell Biol.* **79,** 168–180 CrossRef Medline
28. Colaianni, G., Lippo, L., Sanesi, L., Brunetti, G., Celi, M., Cirulli, N., Passeri, G., Reseland, J., Schipani, E., Faienza, M. F., Tarantino, U., Colucci, S., and Grano, M. (2018) Deletion of the transcription factor PGC-1α in mice negatively regulates bone mass. *Calcif. Tissue Int.* **103,** 638–652 CrossRef Medline
29. Arnett, T. R., and Orriss, I. R. (2018) Metabolic properties of the osteoclast. *Bone* **115,** 25–30 CrossRef Medline
30. Indo, Y., Takeshita, S., Ishii, K.-A., Hoshii, T., Aburatani, H., Hirao, A., and Ikeda, K. (2013) Metabolic regulation of osteoclast differentiation and function. *J. Bone Miner. Res.* **28,** 2392–2399 CrossRef Medline
31. Larsen, K. I., Falany, M. L., Ponomareva, L. V., Wang, W., and Williams, J. P. (2002) Glucose-dependent regulation of osteoclast H^+-ATPase expression: potential role of p38 MAP-kinase. *J. Cell Biochem.* **87,** 75–84 CrossRef Medline
32. Papanicolaou, K. N., Kikuchi, R., Ngoh, G. A., Coughlan, K. A., Dominguez, I., Stanley, W. C., and Walsh, K. (2012) Mitofusins 1 and 2 are essential for postnatal metabolic remodeling in heart. *Circ. Res.* **111,** 1012–1026 CrossRef Medline
33. Larrea, D., Pera, M., Gonnelli, A., Quintana-Cabrera, R., Akman, H. O., Guardia-Laguarta, C., Velasco, K. R., Area-Gomez, E., Dal Bello, F., De Stefani, D., Horvath, R., Shy, M. E., Schon, E. A., and Giacomello, M. (2019) MFN2 mutations in Charcot-Marie-Tooth disease alter mitochondria-associated ER membrane function but do not impair bioenergetics. *Hum. Mol. Genet.* **28,** 1782–1800 CrossRef Medline
34. Hogan, P. G., Chen, L., Nardone, J., and Rao, A. (2003) Transcriptional regulation by calcium, calcineurin, and NFAT. *Genes Dev.* **17,** 2205–2232 CrossRef Medline
35. Naon, D., Zaninello, M., Giacomello, M., Varanita, T., Grespi, F., Lakshminaranayan, S., Serafini, A., Semenzato, M., Herkenne, S., Hernández-Alvarez, M. I., Zorzano, A., De Stefani, D., Dorn, G. W., 2nd, and Scorrano, L. (2016) Critical reappraisal confirms that Mitofusin 2 is an endoplasmic reticulum-mitochondria tether. *Proc. Natl. Acad. Sci. U.S.A.* **113,** 11249–11254 CrossRef Medline
36. Kowaltowski, A. J., Menezes-Filho, S. L., Assali, E. A., Gonçalves, I. G., Cabral-Costa, J. V., Abreu, P., Miller, N., Nolasco, P., Laurindo, F. R. M., Bruni-Cardoso, A., and Shirihai, O. S. (2019) Mitochondrial morphology regulates organellar Ca^{2+} uptake and changes cellular Ca^{2+} homeostasis. *FASEB J.* **33,** 13176–13188 CrossRef Medline
37. Jung, S., Kwon, J.-O., Kim, M. K., Song, M.-K., Kim, B., Lee, Z. H., and Kim, H.-H. (2019) Mitofusin 2, a mitochondria-ER tethering protein, facilitates osteoclastogenesis by regulating the calcium-calcineurin-NFATc1 axis. *Biochem. Biophys. Res. Commun.* **516,** 202–208 CrossRef Medline
38. Decker, C. E., Yang, Z., Rimer, R., Park-Min, K.-H., Macaubas, C., Mellins, E. D., Novack, D. V., and Faccio, R. (2015) Tmem178 acts in a novel negative feedback loop targeting NFATc1 to regulate bone mass. *Proc. Natl. Acad. Sci. U.S.A.* **112,** 15654–156549 CrossRef Medline
39. Yang, Z., Yan, H., Dai, W., Jing, J., Yang, Y., Mahajan, S., Zhou, Y., Li, W., Macaubas, C., Mellins, E. D., Shih, C.-C., Fitzpatrick, J. A. J., and Faccio, R. (2019) Tmem178 negatively regulates store-operated calcium entry in myeloid cells via association with STIM1. *J. Autoimmun.* **101,** 94–108 CrossRef Medline
40. Boutant, M., Kulkarni, S. S., Joffraud, M., Ratajczak, J., Valera Alberni, M., Combe, R., Zorzano, A., and Cantó, C. (2017) Mfn2 is critical for brown adipose tissue thermogenic function. *EMBO J.* **36,** 1543–1558 CrossRef Medline
41. Mahdaviani, K., Benador, I. Y., Su, S., Gharakhanian, R. A., Stiles, L., Trudeau, K. M., Cardamone, M., Enríquez-Zarralanga, V., Ritou, E., Aprahamian, T., Oliveira, M. F., Corkey, B. E., Perissi, V., Liesa, M., and Shirihai, O. S. (2017) Mfn2 deletion in brown adipose tissue protects from insulin resistance and impairs thermogenesis. *EMBO Rep.* **18,** 1123–1138 CrossRef Medline
42. Chen, Y., Liu, Y., Dorn, G. W., 2nd (2011) Mitochondrial fusion is essential for organelle function and cardiac homeostasis. *Circ. Res.* **109,** 1327–1331 CrossRef Medline
43. Papanicolaou, K. N., Khairallah, R. J., Ngoh, G. A., Chikando, A., Luptak, I., O'Shea, K. M., Riley, D. D., Lugus, J. J., Colucci, W. S., Lederer, W. J., Stanley, W. C., and Walsh, K. (2011) Mitofusin-2 maintains mitochondrial structure and contributes to stress-induced permeability transition in cardiac myocytes. *Mol. Cell Biol.* **31,** 1309–1328 CrossRef Medline
44. Shen, T., Zheng, M., Cao, C., Chen, C., Tang, J., Zhang, W., Cheng, H., Chen, K.-H., and Xiao, R.-P. (2007) Mitofusin-2 is a major determinant of oxidative stress-mediated heart muscle cell apoptosis. *J. Biol. Chem.* **282,** 23354–23361 CrossRef Medline
45. Chen, H., McCaffery, J. M., and Chan, D. C. (2007) Mitochondrial fusion protects against neurodegeneration in the cerebellum. *Cell* **130,** 548–562 CrossRef Medline
46. Clausen, B. E., Burkhardt, C., Reith, W., Renkawitz, R., and Förster, I. (1999) Conditional gene targeting in macrophages and granulocytes using LysMcre mice. *Transgenic Res.* **8,** 265–277 CrossRef Medline
47. Nazarian, A., Snyder, B. D., Zurakowski, D., and Müller, R. (2008) Quantitative micro-computed tomography: a non-invasive method to assess equivalent bone mineral density. *Bone* **43,** 302–311 CrossRef Medline
48. Bouxsein, M. L., Boyd, S. K., Christiansen, B. A., Guldberg, R. E., Jepsen, K. J., and Müller, R. (2010) Guidelines for assessment of bone microstructure in rodents using micro-computed tomography. *J. Bone Miner. Res.* **25,** 1468–1486 CrossRef Medline
49. Dempster, D. W., Compston, J. E., Drezner, M. K., Glorieux, F. H., Kanis, J. A., Malluche, H., Meunier, P. J., Ott, S. M., Recker, R. R., and Parfitt, A. M. (2013) Standardized nomenclature, symbols, and units for bone histomorphometry: a 2012 update of the report of the ASBMR Histomorphometry Nomenclature Committee. *J. Bone Miner. Res.* **28,** 2–17 Medline
50. Takeshita, S., Kaji, K., and Kudo, A. (2000) Identification and characterization of the new osteoclast progenitor with macrophage phenotypes being able to differentiate into mature osteoclasts. *J. Bone Miner. Res.* **15,** 1477–1488 CrossRef Medline
51. Morita, S., Kojima, T., and Kitamura, T. (2000) Plat-E: an efficient and stable system for transient packaging of retroviruses. *Gene Ther.* **7,** 1063–1066 CrossRef Medline
52. Zou, W., Deselm, C. J., Broekelmann, T. J., Mecham, R. P., Vande Pol, S., Choi, K., and Teitelbaum, S. L. (2012) Paxillin contracts the osteoclast cytoskeleton. *J. Bone Miner. Res.* **27,** 2490–2500 CrossRef Medline
53. Shashkova, E. V., Trivedi, J., Cline-Smith, A. B., Ferris, C., Buchwald, Z. S., Gibbs, J., Novack, D., and Aurora, R. (2016) Osteoclast-primed Foxp3+ CD8 T cells induce T-bet, eomesodermin, and IFN-γ to regulate bone resorption. *J. Immunol.* **197,** 726–735 CrossRef Medline